Feedback Control of the Contour Shape in Heavy-Plate Hot Rolling

Feedback control of the contour shape in heavy-plate hot rolling

F. Schausberger, A. Steinboeck, and A. Kugi

***Abstract*—This paper deals with mathematical modeling and feedback control of the contour evolution in heavy-plate rolling. During the rolling process, asymmetric rolling conditions in the lateral direction may lead to a deviation between the actual and the desired plate contour. Such asymmetric rolling conditions are often unknown and hence cannot be compensated in advance. Therefore, a feedback control approach to reduce contour errors during the rolling process is presented. However, the measurement of the plate contour is subject to a transport delay which complicates the design of feedback controllers. The angular velocity of the plate is also linked with its contour evolution. This is why the delay-free measurement of the angular movement is used in a 2-DOF Smith-predictor structure. The basis for the control approach is a mathematical model describing the nexus between the angular velocity and the contour evolution of the plate. The feedback controller utilizes an upstream and a downstream measurement of the contour and the movement of the plate. Furthermore, a proof of the robust stability of the proposed control concept is presented. Simulation results and measurements from an industrial plant demonstrate that the presented approach can significantly reduce the contour errors of rolled plates.**

***Index Terms*—Shape control of heavy plates, Heavy plate rolling mill, Snaking, Smith-predictor, Model-based control, Feedback control**

I. Introduction

IN the production of heavy plates, the thickness is successively reduced to a desired plate thickness using heavy-plate rolling mills (cf. Fig. 1). A single reduction of the plate thickness is called pass or rolling pass and is typically performed in alternating direction at reversing mill stands. The head end of the plate is the first part of the plate to leave the rolling gap, whereas the tail end passes the rolling gap at the end of the pass. The quality of the final product is mainly characterized by the material properties, the shape and the thickness of the plate. The usable area after edge trimming clearly depends on the shape of the plate. Hence, the resulting plate contour is of special interest in the production process. Imperfections of the plate contour may result from asymmetric rolling conditions in the lateral direction of the plate. This includes inhomogeneous input and/or output thickness profiles in the width direction and spatially inhomogeneous as well as time-dependent temperature variations of the plate. These are the motivations for the development of controllers which improve the shape of the rolled products, in particular the plate contour. Asymmetric rolling conditions in the lateral direction are often unknown and cannot be compensated in advance to

The authors are with the Automation and Control Institute, TU Wien, 1040 Vienna, Austria (e-mail: {schausberger,steinboeck,kugi}@acin.tuwien.ac.at)

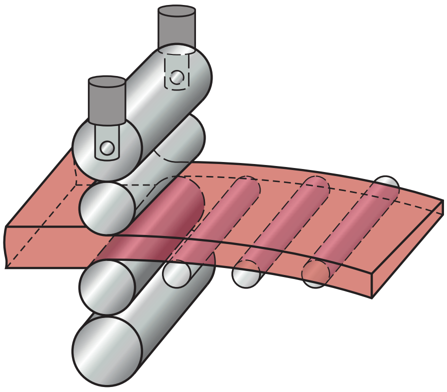

Fig. 1. 4-high rolling mill and contour error (camber) appearing during the rolling process.

prevent the plate from camber. Hence, a common approach is to apply feedback if contour errors appear. Such approaches require a measurement of the plate contour. Furthermore, the camber formation has to be understood to be able to calculate the necessary control inputs to the mill stand. For this calculation, mathematical models covering the evolution of the contour and the movement of the plate may be used. As the considered contour errors are caused by asymmetric rolling conditions, a common countermeasure is to use asymmetric rolling gap profiles in the range of a few hundredths of a millimeter. The resulting non-homogeneous deformation in the rolling gap may lead to a rotation of the plate as discussed in [1].

The angular velocity is linked with the lateral movement (snaking) of the plate in the rolling gap. This movement may lead to an off-center position of the plate in the lateral direction. Because of the resulting asymmetric loading of the roll stack, knowledge of the lateral position of the plate is also vital for the necessary adjustment of the rolling gap actuators.

Moveable side guides are installed before and after the considered mill stand, which center the plate in the lateral direction before each rolling pass. During the rolling pass, the downstream side guides are opened at their outermost position. The upstream side guides can also be used to center the plates which would otherwise move sidewards during the rolling pass.

A. Existing solutions

The literature offers different approaches for the measurement of the contour and the lateral position of heavy plates

Post-print version of the article: F. Schausberger, A. Steinboeck, and Kugi, "Feedback control of the contour shape in heavy-plate hot rolling," *IEEE Transactions on Control Systems Technology*, vol. 26, no. 3, pp. 842–856, 2018. DOI: 10.1109/TCST.2017.2695168
The content of this post-print version is identical to the published paper but without the publisher's final layout or copy editing.

and strips (flat products) during the rolling process. In hot strip rolling, several consecutive mill stands reduce the thickness of the strip. Thereby, mainly the lateral position and the movement of the product during the rolling process are of interest. In heavy-plate rolling, the plate contour is also of interest and should thus be measured.

Mainly 2D visible-light or infrared cameras are used as measurement devices in the published approaches. A common approach is to detect the edges of the processed material within the bitmaps by means of an appropriate edge detection algorithm, see, e.g., [2]. The lateral position of a strip can be directly calculated from the detected edges, see, e.g., [3]. If the heavy plate fits into a single image, the measurement of the contour is equivalent to the detection of the plate edges, see, e.g., [4] and [5].

In general, a heavy plate cannot be captured within a single image because the plate may be long and partly hidden by other plant components. Hence, the camera can only capture parts of the rolled plate and the contour has to be determined using a series of images. A method to join the detected edges of neighboring images based on the longitudinal speed of the plate and to ensure C_1-continuity is presented in [6]. Algorithms that stitch together several images of the plate are addressed in [7]–[9]. Common feature points are identified on two consecutive images to determine the relative displacement between the images from a CCD camera.

Several approaches for modeling of the contour evolution and the movement of plates and strips in hot rolling may be found in literature. In [1] and [10], models only utilizing the continuity of mass in the rolling gap to predict the evolution of the strip centerline are presented. Soaring computer performance facilitates complex models that capture the elastoplastic deformation of the rolled material and the elastic deformation of the mill stand by means of the finite element method (FEM), see, e.g., [11]–[15].

The problem of steering control in hot strip rolling is addressed in [16]–[21] with control concepts ranging from simple PID-control to model predictive control. Control strategies for the reduction of contour errors in heavy-plate rolling are barely discussed in literature. An early control-based approach for the reduction of contour errors is addressed in [22]. A model linking the thickness asymmetry in the lateral direction with the resulting camber and a setup to measure the camber of the plate are presented. The camber of the plate is measured in the forward pass and the asymmetry of the rolling gap is adjusted in the backward pass to reduce the camber.

A three-dimensional FEM simulation for the hot rolling of heavy plates is presented in [23]. The rolls of the mill stand are assumed to be rigid and the plate is treated as a rigid perfectly plastic body. The simulation is used to design an output feedback fuzzy controller to control the camber and the lateral movement of the plate during the rolling pass by adjusting the rolling gap asymmetry. Simulation results show that the presented feedback controller outperforms simple PI-control.

B. Motivations and objectives of this work

The camber reducing approaches found in literature do not fully exploit the capabilities resulting from the alternating rolling direction during heavy-plate rolling. The subsequent rolling passes on reversing mill stands offer the use of two different control strategies:

- Use the measurement of the plate contour to curb occurring camber in the subsequent pass(es).
- Measure the plate contour and counteract to contour errors during the same pass.

Devices to measure the plate contour cannot be installed right next to the rolling gap but in a certain distance from the mill stand. This distance induces a time delay (transport delay) between the generation of the plate contour in the rolling gap and the contour measurement. Hence all appearing contour errors can only be corrected with a delay. Therefore, a feedforward compensation of contour errors from one pass to the subsequent pass (see, e.g., [24]) seems suitable.

Despite a feedforward controller, imperfections like disturbances, model-plant mismatches, or inaccurate rolling gap control may lead to a deviation between the required and the actual output thickness profile and hence to a deviation between the desired and the resulting contour. In particular during the last rolling pass, no further correction of the contour is possible with a feedforward approach. Hence, an additional feedback controller seems favorable to reduce contour errors emerging during the current rolling pass.

The measurement of the plate contour used for feedback control should be as near as possible to the rolling gap to keep the transport delay between camber generation and camber measurement small. Directly at the mill stand, the harsh environment may deteriorate the accuracy and the robustness of measurements. Furthermore, the plate is covered by the rolling mill nearby the rolling gap. Hence, the contour can only be measured at a certain distance from the rolling gap. At the considered rolling mill, the fields of view of the cameras that capture the plate contour are located 5 m away from the rolling gap. Clearly, the resulting transport delay of the measured plate contour in general complicates the use of feedback controllers. Nevertheless, the transport delay and its effect on feedback control are generally not addressed in the literature on camber control.

This is why a feedback control approach utilizing the measurement of both the angular velocity and the contour of the plate is developed in this work. It is shown that the angular velocity of the plate is linked with the contour evolution. The measurement of the angular velocity is not subject to a transport delay and is therefore utilized in the presented feedback control approach. In particular, a 2-DOF Smith-predictor, i.e., a combination of a feedforward controller and a feedback Smith-predictor controller, is used. A prerequisite of the presented feedback control approach is that in addition to the plate contour also the angular movement of the plate can be measured. However, most of the contour measurement approaches found in literature do not cover the measurement of the plate movement. Hence, the measurement approach presented in [25] is used. It features a contour and movement

Post-print version of the article: F. Schausberger, A. Steinboeck, and Kugi, "Feedback control of the contour shape in heavy-plate hot rolling," *IEEE Transactions on Control Systems Technology*, vol. 26, no. 3, pp. 842–856, 2018. DOI: 10.1109/TCST.2017.2695168
The content of this post-print version is identical to the published paper but without the publisher's final layout or copy editing.

measurement tailored to feedback control. The output of the feedback controller is added to the output of the pass-to-pass based feedforward control presented in [24]. The feedforward controller uses the measurement of the plate contour after a rolling pass to determine the necessary asymmetry of the rolling gap which yields the desired plate contour after the subsequent rolling pass. This combination of the pass-to-pass feedforward control and the feedback control should help to fully utilize the alternating rolling direction in heavy-plate rolling for the reduction of contour errors.

C. Overview of the control approach

Fig. 2 shows an overview of the proposed control system. To measure the contour during the rolling pass, two infrared cameras are installed at the ceiling of the rolling mill, one before and one after the mill stand. This configuration allows to measure the contour and the angular velocity of the plate both upstream and downstream of the rolling gap. The evolution of the downstream contour also depends on the upstream movement and contour of the plate. Hence, the measurements of both cameras are used in the proposed feedback controller to effectively reduce contour errors. Feedforward control is applied in every pass with a valid plate contour measurement obtained during the previous pass. The feedback controller is always activated when the plate length exceeds a certain value because almost no improvement of the contour can be achieved by feedback for short plates.

The outputs of the feedback and the feedforward controller are added and then sent to the automation system of the mill stand.

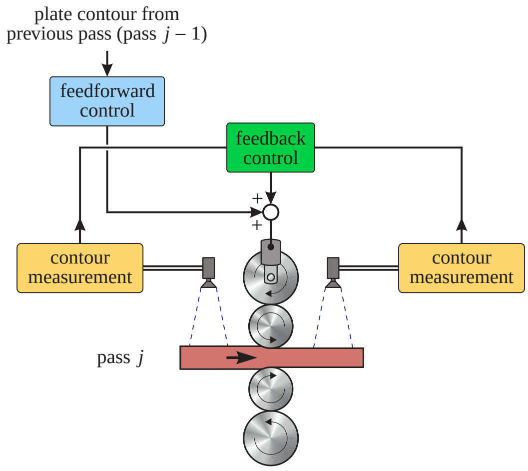

Fig. 2. Downstream and upstream contour measurement in combination with feedforward and feedback control.

D. Structure of the paper

The paper is organized as follows: Section II very briefly summarizes the method from [25] that determines the contour and the angular velocity of the plate. A mathematical model of the contour evolution and the movement of the plate is discussed and validated in Section III. Based on this model, a feedback controller to reduce camber is presented in Section IV. Furthermore, the robust stability of the proposed control concept is shown. Simulation results and measurements shown in Section V demonstrate the feasibility of the proposed method. Section VI concludes the work with a summary.

II. Measurement of the plate contour and the plate movement

The proposed feedback control approach essentially requires the measurement of the plate contour and the movement (angular and translational velocity) of the plate. These requirements are fulfilled by the contour and velocity measurement approaches presented in [25] and [26]. In these approaches, infrared 2D-CCD cameras are used to capture the plate. For the considered application, infrared cameras are superior compared to standard visible light cameras due to several reasons. First of all, hot objects can be also captured through a cloud of steam and due to the high thermal contrast between the plate and its environment further illumination is not needed. Furthermore, infrared cameras are not subject to disturbing light sources in contrast to visible light cameras, where, e.g., sun light can be a problem.

Often, the whole plate contour cannot be captured by a single image because the plate may be long and partly covered by other plant components. Furthermore, the measurement has to be continuously repeated during the rolling pass for feedback control. Hence, the camera only captures parts of the rolled plate and the contour has to be determined using a series of consecutive images. The edges are detected in the bitmaps with a threshold-based edge detection algorithm and then used to estimate a polynomial representation of the longitudinal plate boundaries. The optimization-based moving-horizon estimator considers the restrictions of the movement of the plate, i.e. that the plate is clamped in the rolling gap. The measurement outputs are the plate contour (longitudinal and lateral edges) and the angular velocity of the plate. Furthermore, the longitudinal velocity can be estimated by the presented approach as long as the head or tail end of the plate is in the field of view (FOV) of the camera. A measurement of the longitudinal velocity is necessary for the whole rolling pass. This is why the velocity is estimated by means of the approach presented in [26] which utilizes the generally non-uniform temperature field of the plate (cf. Fig. 3).

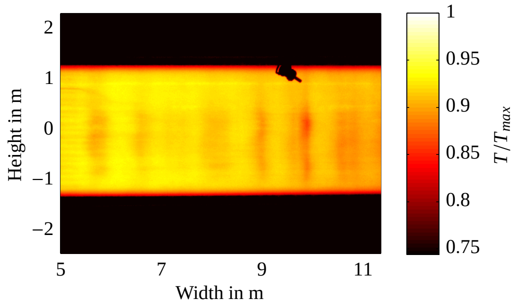

Fig. 3. Thermographic image of a heavy plate with a spatially fixed disturbance (pyrometer).

Post-print version of the article: F. Schausberger, A. Steinboeck, and Kugi, “Feedback control of the contour shape in heavy-plate hot rolling,” *IEEE Transactions on Control Systems Technology*, vol. 26, no. 3, pp. 842–856, 2018. doi: 10.1109/TCST.2017.2695168
The content of this post-print version is identical to the published paper but without the publisher’s final layout or copy editing.

These inhomogeneities may be caused by non-uniform heating in the slab furnace or inhomogeneous conditions during the rolling process and are in general unfavorable. However, they are advantageous in terms of the used velocity estimation.

III. Modeling of the plate movement

In the following, a tailored mathematical model covering the plate movement and the evolution of the plate contour is described. This model is based on some kinematic assumptions and the continuity equation. The model is the basis for an online feedback control approach utilizing measurements of the plate contour and the angular velocity of the plate up- and downstream of the mill stand. Fig. 4 shows a top view of the mill stand with the global coordinate frame (ξ, η, ζ) (Eulerian coordinates). It is assumed that the material flow in the rolling gap is strictly perpendicular to the work roll axis, which implies that lateral spread of the plate in the rolling gap is neglected. The camber characterized by the lateral displacement $\delta(\xi)$ of the centerline of the plate is of interest (cf. Fig. 4). The displacement $\delta(\xi)$ is the arithmetical mean of the coordinates η of the longitudinal boundaries of the plate. Clearly, $\delta(\xi)$ is a function of the time t because of the motion and the deformation of the plate. For the sake of readability, the argument t is omitted in the following. The centerline $\delta(\xi)$

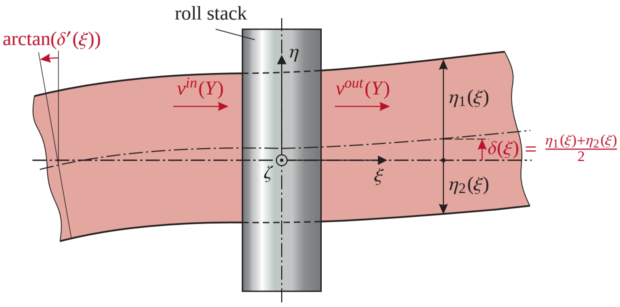

Fig. 4. Top view of the rolling process.

can be computed based on the contour measurement. The local slope $\delta'(\xi)$ of the centerline (with respect to the axis ξ) is

$$\delta'(\xi) = \frac{\partial \delta(\xi)}{\partial \xi}$$

and the local curvature $\delta''(\xi)$ follows in the form

$$\delta''(\xi) = \frac{\frac{\partial^2 \delta(\xi)}{\partial \xi^2}}{\left(1 + \left(\frac{\partial \delta(\xi)}{\partial \xi}\right)^2\right)^{\frac{3}{2}}} \approx \frac{\partial^2 \delta(\xi)}{\partial \xi^2}. \tag{1}$$

Because the local slope $\delta'(\xi)$ is expected to be very small the curvature $\delta''(\xi)$ can be approximated by $\partial^2\delta(\xi)/\partial\xi^2$.

A. Movement of the plate

In the following, a kinematic model of the movement of the plate based on the continuity equation in the rolling gap is derived. The model describes the effects of changing the lateral asymmetry of the input thickness and the rolling gap on the movement of the plate.

Consider the Lagrangian coordinate

$$Y = \eta - \delta(\xi)$$

which points along the direction η because the influence of the very small local slope $\delta'(\xi)$ on the Lagrangian coordinate Y can be neglected. $Y = 0$ holds at the centerline of the plate and $Y = \pm w/2$ defines the boundaries of the plate, with w as the width of the plate. Neglecting any bending deflection or crown of the work rolls, the rolling gap height can be formulated as

$$h^{out}(Y) = \bar{h}^{out} + \tilde{h}^{out}(Y) = \bar{h}^{out} + \Delta h^{out}\frac{Y}{w}, \tag{2}$$

which implies $\bar{h}^{out} = \left(h^{out}(w/2) + h^{out}(-w/2)\right)/2$ and $\Delta h^{out} = h^{out}(w/2) - h^{out}(-w/2)$. In the same way, the input thickness at $\xi = 0$ is parameterized in the form

$$h^{in}(Y) = \bar{h}^{in} + \tilde{h}^{in}(Y) = \bar{h}^{in} + \Delta h^{in}\frac{Y}{w}. \tag{3}$$

The plate enters the rolling gap with the velocity $v^{in}(Y)$ and leaves it with the velocity $v^{out}(Y)$. These two velocities are linked at the point $\xi = 0$ by the continuity equation

$$v^{in}(Y)h^{in}(Y) = v^{out}(Y)h^{out}(Y). \tag{4}$$

Specialization of (4) for $Y = 0$ yields

$$\bar{v}^{in}\bar{h}^{in} = \bar{v}^{out}\bar{h}^{out} \tag{5}$$

with the spatial mean values $\bar{v}^{in}$ and $\bar{v}^{out}$ of the upstream and downstream velocities $v^{in}(Y)$ and $v^{out}(Y)$, respectively. Because there are no external loads outside the rolling gap, the motion of the plate can be characterized as a rigid-body displacement both upstream and downstream of the rolling gap. Due to the assumption of zero material flow along the lateral direction η in the rolling gap, the upstream plate velocity $v^{in}(Y)$ is given by

$$v^{in}(Y) = \bar{v}^{in} - Y\omega^{in}$$

and the downstream plate velocity $v^{out}(Y)$ by

$$v^{out}(Y) = \bar{v}^{out} - Y\omega^{out}.$$

The upstream mean translational velocity follows in the form

$$\bar{v}^{in} = \frac{v^{in}(-w/2) + v^{in}(w/2)}{2}$$

and the upstream angular velocity is

$$\omega^{in} = \frac{v^{in}(-w/2) - v^{in}(w/2)}{w}$$

with respect to the axis ζ at the origin. Similarly, the downstream mean translational velocity follows in the form

$$\bar{v}^{out} = \frac{v^{out}(-w/2) + v^{out}(w/2)}{2}$$

and the downstream angular velocity is

$$\omega^{out} = \frac{v^{out}(-w/2) - v^{out}(w/2)}{w}. \tag{6}$$

Post-print version of the article: F. Schausberger, A. Steinboeck, and Kugi, “Feedback control of the contour shape in heavy-plate hot rolling,” *IEEE Transactions on Control Systems Technology*, vol. 26, no. 3, pp. 842–856, 2018. doi: 10.1109/TCST.2017.2695168
The content of this post-print version is identical to the published paper but without the publisher’s final layout or copy editing.

From (5) the mean velocity of the downstream plate reads as $\bar{v}^{out} = \bar{v}^{in}\bar{h}^{in}/\bar{h}^{out}$. The local velocity of the downstream plate follows from (4) in the form

$$v^{out}(Y) = v^{in}(Y)\frac{\bar{h}^{in} + \Delta h^{in}\frac{Y}{w}}{\bar{h}^{out} + \Delta h^{out}\frac{Y}{w}}, \tag{7}$$

where (2) and (3) have been inserted. The asymmetry of the input thickness and the asymmetry of the rolling gap height are expected to be small compared to their mean values. Therefore, it is reasonable to linearize (7) at the point $\Delta h^{in} = \Delta h^{out} = 0$ resulting in

$$v^{out}(Y) \approx \left(\bar{v}^{in} - Y\omega^{in}\right)\left(\frac{\bar{h}^{in}}{\bar{h}^{out}} + \frac{Y}{w\bar{h}^{out}}\Delta h^{in} - \frac{\bar{h}^{in}Y}{w\left(\bar{h}^{out}\right)^2}\Delta h^{out}\right). \tag{8}$$

Insertion of (8) into (6) yields

$$\omega^{out} = \frac{\bar{v}^{in}}{w}\left(\frac{\bar{h}^{in}}{\left(\bar{h}^{out}\right)^2}\Delta h^{out} - \frac{1}{\bar{h}^{out}}\Delta h^{in}\right) + \frac{\bar{h}^{in}}{\bar{h}^{out}}\omega^{in}. \tag{9}$$

That is, the angular velocity ω^{out} of the downstream plate depends on the velocities of the upstream plate ($\bar{v}^{in}$ and ω^{in}) and the input and output thickness of the plate. Here, a model of the forward and backward slip, see, e.g., [27] and [28], is not needed because the upstream as well as the downstream longitudinal and angular velocities are assumed to be measurable.

B. Evolution of the camber

The evolution of the camber defined in terms of the plate curvature $\delta''(\xi)$ and its nexus with the angular velocities ω^{in} and ω^{out} of the plate are analyzed in the following. The objective of this analysis is to explore whether the camber can be computed based on the measurement of the angular velocities ω^{in} and ω^{out} and the longitudinal velocities $\bar{v}^{in}$ and $\bar{v}^{out}$ of the plate according to Sec. II. If the machine vision system is directly used for camber measurement of the part of the plate that is currently in the FOV of the camera, there is an inherent transport delay between camber generation and camber measurement. This delay is clearly undesirable for feedback control of the camber. However, this delay can be avoided by using measurements of the angular velocity of the plate.

The plate enters the rolling gap with the curvature $\left(\delta^{in}\right)'' = \delta''(0^-)$ and leaves it with the curvature $(\delta^{out})'' = \delta''(0^+)$. Because of the very small expected slope of the centerline $\delta'(\xi)$, the angle $\varphi(\xi) = \arctan(\delta'(\xi))$ of the centerline may be approximated by $\varphi(\xi) = \delta'(\xi)$ and the angular velocity of the material follows in the form

$$\underbrace{\frac{\mathrm{d}\varphi(\xi,t)}{\mathrm{d}t}}_{\omega} = \frac{\partial\delta'(\xi)}{\partial t} + \frac{\delta'(\xi)}{\partial\xi}\underbrace{\frac{\mathrm{d}\xi}{\mathrm{d}t}}_{v}.$$

Hence, the angle $\delta'(0)$ changes according to

$$\frac{\partial\delta'(0^-)}{\partial t} + \left(\delta^{in}\right)''\bar{v}^{in} = \omega^{in} \tag{10a}$$

$$\frac{\partial\delta'(0^+)}{\partial t} + \left(\delta^{out}\right)''\bar{v}^{out} = \omega^{out}. \tag{10b}$$

Because of the thickness reduction $\bar{h}^{out}/\bar{h}^{in}$ in the rolling gap at $Y = 0$ and the associated elongation of the plate, the downstream slope $\delta'(0^+)$ follows in the form

$$\delta'(0^+) = \frac{\bar{h}^{out}}{\bar{h}^{in}}\delta'(0^-). \tag{11}$$

Hence, the derivatives $\delta'(\xi)$ and $\delta''(\xi)$ can be discontinuous at $\xi = 0$. In the following, it is considered that $\bar{h}^{out}/\bar{h}^{in}$ is constant. Elimination of $\delta'(0^-)$ and $\delta'(0^+)$ in (10) and (11) and insertion of (5) yields

$$\left(\delta^{out}\right)'' = \frac{\omega^{out}}{\bar{v}^{out}} - \frac{\bar{h}^{out}}{\bar{h}^{in}}\frac{\omega^{in}}{\bar{v}^{out}} + \left(\frac{\bar{h}^{out}}{\bar{h}^{in}}\right)^2\left(\delta^{in}\right)'', \tag{12}$$

i.e., a relation between the angular velocities ω^{in} and ω^{out} and the curvature of the plate before and after the rolling gap.

C. Time-free formulation

So far, most of the quantities have been parameterized in terms of the time t. This implies that the dynamical behavior depends on the plate velocities $\bar{v}^{in}$ and $\bar{v}^{out}$, which can vary, e.g., if the rotational speed of the work roll changes. Hence, the dynamical model is generally time variant and the transport delay between the mill stand and some downstream curvature measurement device can entail time delays of various lengths. These drawbacks can be circumvented if the processed downstream plate length is used as an independent coordinate instead of the time t. Let

$$X(t) = \int_0^t \bar{v}^{out}(\tau)\mathrm{d}\tau \tag{13}$$

be the length of the already rolled part of the plate measured along the direction ξ. More precisely, $X(t)$ is the curvilinear distance from the mill stand to the head end of the plate. During a rolling pass that starts at the time $t = 0$ (head end of the plate enters the rolling gap), $X(t)$ grows from 0 to the plate length. From (13), it follows that

$$\dot{X}(t) = \bar{v}^{out}(t) \tag{14}$$

or equivalently

$$\mathrm{d}X = \bar{v}^{out}(t)\mathrm{d}t.$$

Based on this relation, the angular displacements per unit processed plate length are defined in the form

$$\Omega^{in} = \frac{\omega^{in}}{\bar{v}^{out}} \tag{15a}$$

$$\Omega^{out} = \frac{\omega^{out}}{\bar{v}^{out}}. \tag{15b}$$

Insertion of these relations and (5) into (9) and (12) yields the time-free description of the camber evolution

$$\Omega^{out} = \frac{1}{w\bar{h}^{out}}\Delta h^{out} - \frac{1}{w\bar{h}^{in}}\Delta h^{in} + \frac{\bar{h}^{in}}{\bar{h}^{out}}\Omega^{in} \tag{16a}$$

$$\left(\delta^{out}\right)'' = \Omega^{out} - \frac{\bar{h}^{out}}{\bar{h}^{in}}\Omega^{in} + \left(\frac{\bar{h}^{out}}{\bar{h}^{in}}\right)^2\left(\delta^{in}\right)''. \tag{16b}$$

Note that all variables in (16) can be formulated as functions of the variable X (in lieu of t).

Post-print version of the article: F. Schausberger, A. Steinboeck, and Kugi, "Feedback control of the contour shape in heavy-plate hot rolling," *IEEE Transactions on Control Systems Technology*, vol. 26, no. 3, pp. 842–856, 2018. DOI: 10.1109/TCST.2017.2695168
The content of this post-print version is identical to the published paper but without the publisher's final layout or copy editing.

D. Validation

In the following, the model of the movement of the plate covering the static equations (16) is validated. For the validation of (16a), the input and the output thickness (mean value and asymmetry) of the plate have to be known. The reached tolerances on the mean thickness of the plate are tight and therefore the desired values of the input and output thickness are used for $\bar{h}^{in}$ and $\bar{h}^{out}$. Hence, it is sufficient to measure the asymmetries of the input and output thickness. However, at the considered rolling mill a thickness measurement device is only installed downstream of the mill stand. Therefore, the thickness of the plate and hence the thickness asymmetry can only be measured after every second pass. This is why (16a) cannot be validated by means of measurements.

Contrary, (16b) can be validated because no thickness asymmetries appear in (16b). In the validation, the curvature of the downstream plate is calculated based on (16b) and then compared to the curvature calculated from the measurement of the downstream centerline according to (1). All necessary quantities in the validation are determined by the contour measurement approach from Sec. II. A Savitzky-Golay filter with degree 3 and window length 31 is used to calculate the curvature based on the measurement of the centerline.

The curvature of the upstream plate can be calculated during the contour measurement itself based on the centerline of the already rolled part of the plate. However, the curvature of the downstream plate can only be calculated after the contour measurement at the downstream camera. To this end, the measured plate contour is shifted in time based on the movement of the plate to compensate for the transport delay and to determine the curvature in the rolling gap.

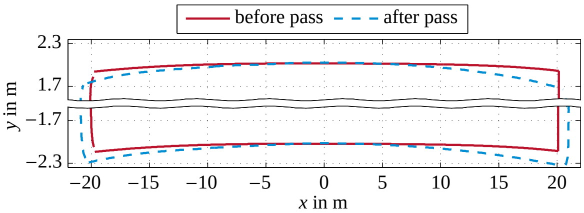

Fig. 5. Contour of the plate before and after the considered rolling pass.

The thickness of the plate used in the validation is reduced from 19.9 mm to 18.5 mm in the considered pass. Fig. 5 shows the measured contours before and after the rolling pass of the plate with a desired plate length of 43.3 m.

Furthermore, Fig. 6 shows the measured upstream and downstream angular displacements as a function of the already rolled plate length X. Only the overlapping part of the angular displacements in Fig. 6 can be used for the validation of (16b). Hence, the measurements of a long plate are used for the validation to have a large overlap.

In this scenario, the upstream angular displacement of the plate is almost zero. This is because the upstream side guides were positioned close to the plate edges to prevent the plate from rotations and from moving sidewards. Contrary, the downstream plate can rotate due to the opened downstream side guides. For rolled plate lengths $X(t)$ larger than approximately 35 m, the plate is no longer between the upstream side guides. This leads to a change of the almost constant downstream angular displacement of the plate (cf. Fig. 6).

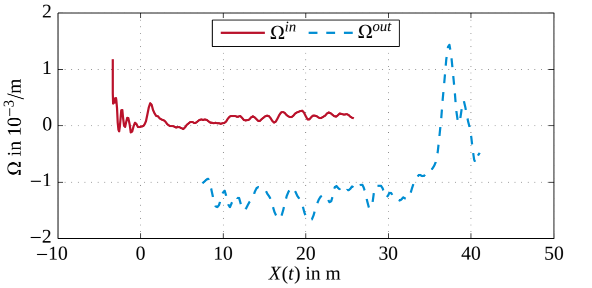

Fig. 6. Measured upstream and downstream angular displacements Ω^{in} and Ω^{out}, respectively.

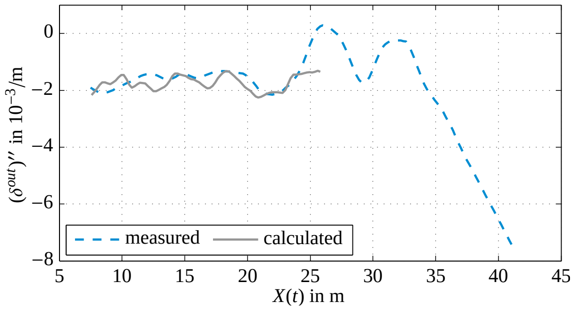

Fig. 7. Measured and calculated downstream curvature of the plate $(\delta^{out})''$.

Fig. 7 shows the measured and the calculated downstream curvature of the considered plate. The mismatch between the measured and the calculated values is in an acceptable range. The missing upstream guidance of the plate for $X \geq 35$ m may also be seen in Fig. 7. It leads to a higher magnitude of the curvature near the end of the plate.

IV. Feedback control during the rolling pass

A non-ideal control of the rolling gap actuators, model-plant mismatches or disturbances may lead to a deviation between the desired and the actual plate contour even if feedforward control is used. Hence, an additional feedback controller is used to (further) improve the contour of the plate. Simple feedback control utilizing the directly measured contour is difficult to apply because of the inherent transport delay between the camber generation in the rolling gap and the camber measurement. To circumvent this difficulty, a control approach using the delay free measurement of the downstream and upstream angular velocities of the plate is presented. The mathematical model of the plate movement from Sec. III is used in the controller design. It describes the nexus between the angular velocity and the resulting curvature of the plate.

A. Plant model

As a preparation step for the feedback controller design, the idealized time-free model (16) is supplemented by an

Post-print version of the article: F. Schausberger, A. Steinboeck, and Kugi, “Feedback control of the contour shape in heavy-plate hot rolling,” *IEEE Transactions on Control Systems Technology*, vol. 26, no. 3, pp. 842–856, 2018. doi: 10.1109/TCST.2017.2695168
The content of this post-print version is identical to the published paper but without the publisher’s final layout or copy editing.

output equation for the measured camber and by disturbances, which may, for instance, be caused by external influences or modeling errors. The inputs of the system are

$$u_1 = \Delta h^{out}, \quad u_2 = \Delta h^{in}, \quad u_3 = \Omega^{in}, \quad u_4 = \left(\delta^{in}\right)''.$$

Here, u_1 is a control input (tilt of the rolling mill) whereas u_2, u_3, and u_4 are externally defined, known inputs. The static model (16) is supplemented by bounded disturbances (process noise) d_1 and d_2 to get the plant model

$$x_1(X) = \Omega^{out} = \frac{1}{w\bar{h}^{out}} \underbrace{\Delta h^{out}}_{u_1(X)} - \frac{1}{w\bar{h}^{in}} \underbrace{\Delta h^{in}}_{u_2(X)} + \frac{\bar{h}^{in}}{\bar{h}^{out}} \underbrace{\Omega^{in}}_{u_3(X)} + d_1(X) \tag{17a}$$

$$x_2(X) = \left(\delta^{out}\right)'' = \underbrace{\Omega^{out}}_{x_1(X)} - \frac{\bar{h}^{out}}{\bar{h}^{in}} \underbrace{\Omega^{in}}_{u_3(X)} + \left(\frac{\bar{h}^{out}}{\bar{h}^{in}}\right)^2 \underbrace{\left(\delta^{in}\right)''}_{u_4(X)} + d_2(X). \tag{17b}$$

In the following, the root cause of these disturbances and their bounds will be described in more detail. The disturbance d_1 is mainly attributed to errors of the asymmetry of the input and output thickness, because the mean thickness $\bar{h}$ and the width w of the plate are well known. From experience the relative error $\Delta h/\bar{h}$ of the thickness asymmetry is in the range of two percent. Hence, it follows that $|d_1| < 2\frac{0.02}{w}$ by assuming the same maximum absolute value 0.02 for the relative error of the asymmetry of the input and output thickness. The disturbance d_2 essentially covers errors of the measurement of Ω^{out}, Ω^{in}, and $\left(\delta^{in}\right)''$. Assuming a relative error of 10 % of each measurement and considering that the curvatures and angular displacements from (17b) are in the range of approximately $1 \cdot 10^{-3}$/m it follows that $|d_2| < 3 \cdot 10^{-4}$/m with $\frac{\bar{h}^{out}}{\bar{h}^{in}} < 1$.

For the controller design it is assumed, that the contour measurement described in Sec. II exactly measures the respective quantities, i.e., without errors. The machine vision system measures the current values $\bar{v}^{in}$, $\bar{v}^{out}$, ω^{in}, and ω^{out} as well as $\delta''(\xi)$ for these parts of the plate that are currently inside the fields of view of the cameras. Therefore, the current (upstream) value $u_4(X) = \left(\delta^{in}\right)''$ is also known from images previously captured by the upstream camera. In contrast, a direct measurement of the current (downstream) value $x_2(X) = (\delta^{out})''$ can only be made by the downstream camera after the plate has traveled the (constant) distance $\xi_{cam} > 0$ from the rolling gap to the field of view of the downstream camera along the direction ξ. This causes a delay between the generation of the camber and its measurement. In the plant model, the camera system is represented by the output equations

$$y_1(X) = x_1(X) \tag{18a}$$

$$y_2(X) = x_2(X - (\xi_{cam} + \tilde{\xi}_{cam})). \tag{18b}$$

Here, ξ_{cam} is the known nominal distance, and $\tilde{\xi}_{cam}$ is the unknown uncertainty of the distance. It is assumed that ξ_{cam} and $\tilde{\xi}_{cam}$ are constant. Because of the unknown disturbances d_1 and d_2 in the (static) process model (17), there is no need to consider extra measurement noise in (18). The output $y_1(X)$ is computed in the measurement system based on (15b) using the measured current values $\bar{v}^{out}$ and ω^{out}.

Note that the process model (17) is a static mapping. The only dynamical behavior of the plant model is the delay in the output equation (18b).

B. Camber control

The model (17) and (18) serves as a basis for the controller design and is rewritten in the compact form

$$x_1(X) = (A_1 + \tilde{A}_1)u_1(X) + (A_2 + \tilde{A}_2)u_2(X) + \frac{1}{A_3 + \tilde{A}_3}u_3(X) + d_1(X) \tag{19a}$$

$$x_2(X) = x_1(X) - (A_3 + \tilde{A}_3)u_3(X) + (A_3 + \tilde{A}_3)^2 u_4(X) + d_2(X) \tag{19b}$$

$$y_1(X) = x_1(X) \tag{19c}$$

$$y_2(X) = x_2(X - (\xi_{cam} + \tilde{\xi}_{cam})) \tag{19d}$$

where the coefficients

$$A_1 + \tilde{A}_1 = \frac{1}{w\bar{h}^{out}} \tag{20a}$$

$$A_2 + \tilde{A}_2 = -\frac{1}{w\bar{h}^{in}} \tag{20b}$$

$$A_3 + \tilde{A}_3 = \frac{\bar{h}^{out}}{\bar{h}^{in}} \tag{20c}$$

are assumed to be constant. $A_i + \tilde{A}_i$ represents the unknown true value of the respective coefficient and A_i is its known nominal counterpart used for all computations. Constancy of these values is a reasonable assumption if $\bar{h}^{in}$ is constant and if the thickness controller ensures $\bar{h}^{out}$ to be constant. This assumption is not necessary for practical control implementation but will simplify the proof of the closed-loop stability. The constants $\tilde{A}_1$, $\tilde{A}_2$, $\tilde{A}_3$, and $\tilde{\xi}_{cam}$ capture the model-plant mismatch and satisfy $|\tilde{A}_1| \ll A_1$, $|\tilde{A}_2| \ll A_2$, $|\tilde{A}_3| \ll A_3$, and $|\tilde{\xi}_{cam}| \ll \xi_{cam}$. They will be of interest in an analysis of the robustness of the controller and are set to zero in the nominal model.

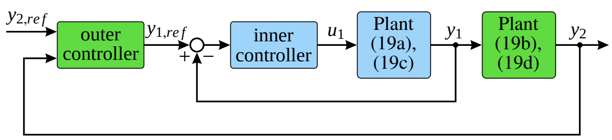

Fig. 8. Cascade structure of the feedback controller.

Fig. 8 shows the proposed cascade control structure with two loops. The inner loop controls $y_1 = \Omega^{out}$ with the control input $u_1 = \Delta h^{out}$, whereas the outer loop uses the control input $y_{1,ref}$ to make $y_2 = (\delta^{out})''$ follow $y_{2,ref}$. As usual for cascade control structures, the inner control loop is assumed to be ideal for the design of the outer control loop.

1) Inner loop : The inner control loop, which controls the plant (19a) and (19c), is outlined in Fig. 9. The control law is formulated as

$$u_1 = u_{1,ff}(X) + u_{1,fb}(X),$$

Post-print version of the article: F. Schausberger, A. Steinboeck, and Kugi, "Feedback control of the contour shape in heavy-plate hot rolling," *IEEE Transactions on Control Systems Technology*, vol. 26, no. 3, pp. 842–856, 2018. DOI: 10.1109/TCST.2017.2695168
The content of this post-print version is identical to the published paper but without the publisher's final layout or copy editing.

where the feedforward part $u_{1,ff}(X)$ is calculated according to [24] and

$$u_{1,fb}(X) = \frac{V_I}{A_1} T_I \left(y_{1,ref}(X) - y_1(X) \right) + \frac{V_I}{A_1} \int_0^X \left(y_{1,ref}(\bar{X}) - y_1(\bar{X}) \right) \mathrm{d}\bar{X} \qquad (21)$$

defines the PI-feedback controller C_I with the controller parameters V_I and T_I. In the feedforward approach (see [24]),

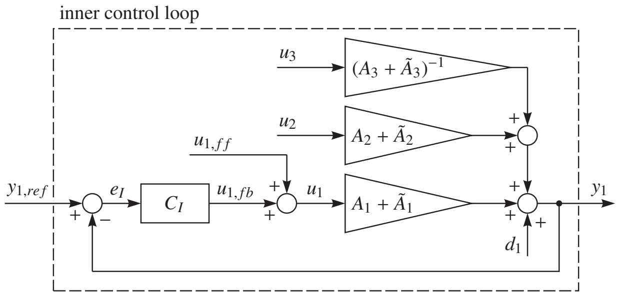

Fig. 9. Inner control loop.

the contour measured after the previous pass is used to determine the necessary adjustment $u_{1,ff}(X)$ of the rolling gap actuators to compensate for the contour error in the actual pass. Herein, a continuum-mechanics model (see [29]) is utilized in an optimization-based approach. As usual for feedforward control, $u_{1,ff}$ can be calculated before the actual pass. In the following, a hat $\hat{}$ labels signals in the Laplace domain and $s \in \mathbb{C}$ is the Laplace variable with the unit 1/m. The transfer function of the PI-feedback controller is

$$C_I(s) = \frac{V_I}{A_1} \frac{1 + sT_I}{s}. \qquad (22)$$

In the Laplace domain, the input-output relation defined by (19a) and (19c) reads as

$$\hat{y}_1(s) = (A_1 + \tilde{A}_1)\hat{u}_1(s) + (A_2 + \tilde{A}_2)\hat{u}_2(s) + \frac{1}{A_3 + \tilde{A}_3}\hat{u}_3(s) + \hat{d}_1(s)$$

and the tracking error (closed-loop control error) follows in the form

$$\begin{aligned} \hat{e}_I(s) &= \hat{y}_{1,ref}(s) - \hat{y}_1(s) \\ &= \frac{1}{1 + (A_1 + \tilde{A}_1)C_I(s)} \Big(\hat{y}_{1,ref}(s) - (A_1 + \tilde{A}_1)\hat{u}_{1,ff}(s) \\ &\quad - (A_2 + \tilde{A}_2)\hat{u}_2(s) - \frac{1}{A_3 + \tilde{A}_3}\hat{u}_3(s) - \hat{d}_1(s) \Big). \end{aligned} \qquad (23)$$

For closed-loop stability, the denominator of (23) must be Hurwitz. Insertion of (22) into (23) shows that this is satisfied if $V_I > 0$ and $V_I T_I > -A_1/(A_1 + \tilde{A}_1) \approx -1$. The scaling $1/A_1$ in the control law (21) results in a closed-loop dynamics independent of w and $\bar{h}^{out}$ for $\tilde{A}_1 = 0$. This property simplifies the choice of the controller parameters V_I and T_I as they do not have to be adjusted to plates with different dimensions. The final value theorem shows that

$$\lim_{X \to \infty} e_I(X) = \lim_{s \to 0} s\hat{e}_I(s) = 0$$

holds for constant inputs $y_{1,ref}$, $u_{1,ff}$, u_2, u_3, and d_1, i.e., the steady-state error vanishes in this case.

2) Outer loop : The outer control loop, which controls the plant (19b) and (19d), is shown in Fig. 10. Here, a 2-DOF Smith-predictor structure, i.e., a combination of a feedforward controller and a feedback Smith-predictor controller is used, see, e.g., [30] and [31]. Because the model in its time-free formulation (16) is used for the controller design, the transport delay of the measurement of the curvature is constant. That is, when using the rolled plate length X as independent coordinate, the transport delay simply represents the distance between the mill stand axis and the measurement device. Clearly, this results in a constant delay of the measurement. Thus, a control approach with a classical Smith-predictor can be applied to the mathematical model (17) and (18) in a straightforward way. For the design and the analysis of robust stability of this loop, the inner loop is assumed to be ideal, which means $y_1 = y_{1,ref}$.

The control law

$$y_{1,ref}(X) = y_{1,ff}(X) + y_{1,fb}(X)$$

with the feedforward controller F_O defined by

$$y_{1,ff}(X) = y_{2,ref}(X + \xi_{cam}) + A_3 u_3(X) - A_3^2 u_4(X) \qquad (24)$$

and the PI-feedback controller defined by

$$y_{1,fb}(X) = V_O T_O \tilde{e}_O(X) + V_O \int_0^X \tilde{e}_O(\bar{X}) \mathrm{d}\bar{X}$$

is used for the outer control loop. The PI-feedback controller of the outer control loop with the parameters T_O and V_O reads as

$$C_O(s) = V_O \frac{1 + sT_O}{s}. \qquad (25)$$

As usual for a Smith-predictor, the input of the feedback controller is defined in the form

$$\begin{aligned} \tilde{e}_O(X) = y_{2,ref}(X) - y_2(X) - \big(& y_1(X) - A_3 u_3(X) + A_3^2 u_4(X) \\ & - y_1(X - \xi_{cam}) + A_3 u_3(X - \xi_{cam}) - A_3^2 u_4(X - \xi_{cam}) \big), \end{aligned}$$

where $y_1(X) - A_3 u_3(X) + A_3^2 u_4(X)$ is the internal model prediction of $x_2(X)$ (cf. (19b)).

In the Laplace domain, the input-output relation defined by (19b) and (19d) reads as

$$\hat{y}_2(s) = \left(\hat{y}_1(s) - \bar{A}_3 \hat{u}_3(s) + \bar{A}_3^2 \hat{u}_4(s) + \hat{d}_2(s) \right) \mathrm{e}^{-s\bar{\xi}_{cam}}$$

with $\bar{\xi}_{cam} = \xi_{cam} + \tilde{\xi}_{cam}$ and $\bar{A}_3 = A_3 + \tilde{A}_3$. The closed-loop transfer function relevant for internal stability can be written utilizing Fig. 10, (24), and (25) in the form

$$\begin{bmatrix} \hat{y}_{1,ref}(s) \\ \hat{y}_2(s) \end{bmatrix} = \mathbf{T}(s) \begin{bmatrix} \hat{y}_{2,ref}(s) \\ \hat{d}_2(s) \\ \hat{u}_3(s) \\ \hat{u}_4(s) \end{bmatrix} \qquad (26)$$

Post-print version of the article: F. Schausberger, A. Steinboeck, and Kugi, "Feedback control of the contour shape in heavy-plate hot rolling," *IEEE Transactions on Control Systems Technology*, vol. 26, no. 3, pp. 842–856, 2018. DOI: 10.1109/TCST.2017.2695168
The content of this post-print version is identical to the published paper but without the publisher's final layout or copy editing.

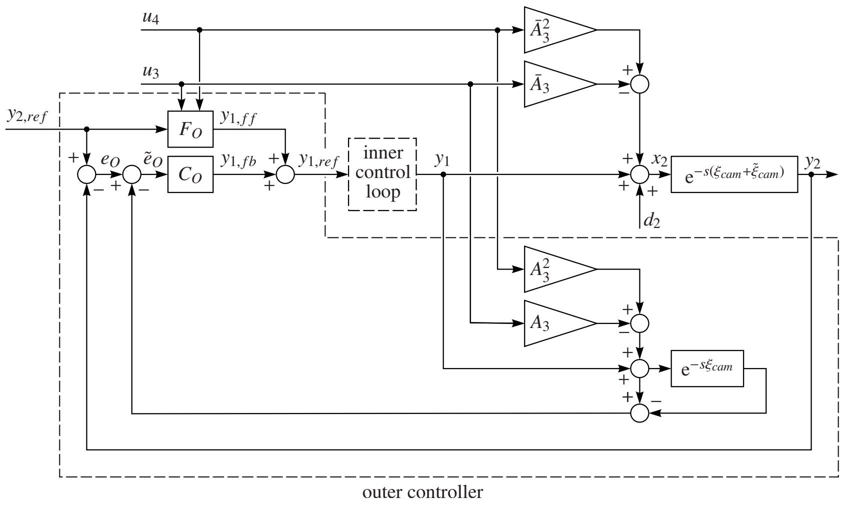

Fig. 10. Outer control loop.

with the matrix

$$
\begin{aligned}
\mathbf{T}(s) &= \frac{1}{1+L(s)}\mathbf{N}(s) \\
&= \frac{1}{1+C_O(s)\left(1+\mathrm{e}^{-s\tilde{\xi}_{cam}}-\mathrm{e}^{-s\xi_{cam}}\right)} \\
&\quad \begin{bmatrix} N_{11}(s) & N_{12}(s) & N_{13}(s) & N_{14}(s) \\ N_{21}(s) & N_{22}(s) & N_{23}(s) & N_{24}(s) \end{bmatrix}
\end{aligned} \tag{27}
$$

and the abbreviations

$$
\begin{aligned}
N_{11}(s) &= C_O(s) + \mathrm{e}^{s\xi_{cam}} \\
N_{12}(s) &= -C_O(s)\mathrm{e}^{-s\tilde{\xi}_{cam}} \\
N_{13}(s) &= A_3 + C_O(s)\left(\tilde{A}_3\mathrm{e}^{-s\tilde{\xi}_{cam}} + A_3(1-\mathrm{e}^{-s\xi_{cam}})\right) \\
N_{14}(s) &= -A_3^2 - C_O(s)\left(\tilde{A}_3^2\mathrm{e}^{-s\tilde{\xi}_{cam}} + A_3^2(1-\mathrm{e}^{-s\xi_{cam}})\right) \\
N_{21}(s) &= \left(C_O(s) + \mathrm{e}^{s\xi_{cam}}\right)\mathrm{e}^{-s\tilde{\xi}_{cam}} \\
N_{22}(s) &= \left(1 + C_O(s)(1-\mathrm{e}^{-s\xi_{cam}})\right)\mathrm{e}^{-s\tilde{\xi}_{cam}} \\
N_{23}(s) &= -\tilde{A}_3 N_{22}(s) \\
N_{24}(s) &= \tilde{A}_3(2A_3+\tilde{A}_3)N_{22}(s).
\end{aligned}
$$

Without any model-plant mismatch and with an exactly known position of the curvature measurement, i.e. $\tilde{A}_3 = 0$ and $\tilde{\xi}_{cam} = 0$, satisfying $V_O > 0$ and $V_O T_O > -1$ ensures the BIBO stability of (26) and thus internal stability of the system. $V_O > 0$ and $V_O T_O > -1$ are assumed throughout this chapter.

In general, the position of the curvature measurement is uncertain, i.e., $\tilde{\xi}_{cam} \neq 0$. The control loop is rearranged as shown in Fig. 11 for the test of internal stability. The task of proving internal stability is to show that the transfer functions between every input/output combination in the closed-loop system of the signals shown in Fig. 11 are BIBO-stable. The signal $y_{1,ff}$ can be shifted and added to u_I and u_O. Furthermore, the signals u_I and u_O can be shifted behind the transfer function blocks $1-\mathrm{e}^{-s\xi_{cam}}$ and $\mathrm{e}^{-s(\xi_{cam}+\tilde{\xi}_{cam})}$, respectively, because these two transfer functions are BIBO-stable. Hence, the effect of u_I and u_O is equivalent to that of $y_{2,ref}$. Consequently, $y_{1,ff}$, u_I, and u_O are not relevant for the stability analysis and are set to zero, i.e., $y_{1,ff} = u_I = u_O = 0$ and it is sufficient to show the stability of the control loop with the reference value $y_{2,ref}$ as input and y_2 as output.

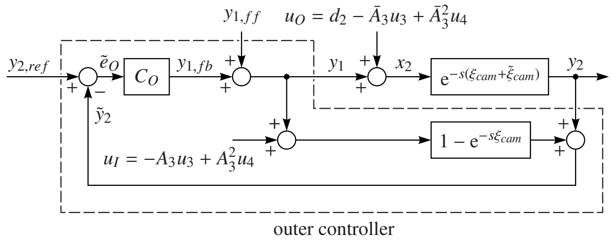

Fig. 11. Proof of robust stability of the outer control loop.

However, it is easier to show the stability for the reference value $y_{2,ref}$ as input and $\tilde{y}_2$ as output because this input/output combination results in a SISO feedback control loop with $L(s)$ in the forward branch and gain 1 in the feedback branch. Proving the stability for $\tilde{y}_2$ is sufficient because when $\tilde{y}_2$ is bounded also y_2 is bounded. The test for internal stability is to analyze whether $\frac{1}{1+L(s)} \in \hat{\mathcal{A}}$, see [32], for all admissible values of $\tilde{\xi}_{cam}$, where $\hat{\mathcal{A}}$ is the set of Laplace transforms of BIBO-stable impulse responses as defined in [32] or [33]. The idea of a Nyquist-like stability test, see, e.g., [33], is used for this analysis which consists of two parts:

First, it must be shown that $L(s)$ can be written in the form

$$
L(s) = L_a(s) + L_r(s),
$$

where $L_a(s) \in \hat{\mathcal{A}}$ and $L_r(s)$ is rational and strictly proper.

Post-print version of the article: F. Schausberger, A. Steinboeck, and Kugi, “Feedback control of the contour shape in heavy-plate hot rolling,” *IEEE Transactions on Control Systems Technology*, vol. 26, no. 3, pp. 842–856, 2018. DOI: 10.1109/TCST.2017.2695168
The content of this post-print version is identical to the published paper but without the publisher’s final layout or copy editing.

Insertion of (25) into $L(s)$ from (27) yields, see also Fig. 11,

$$L(s) = \underbrace{\left(\frac{V_O}{s}\right)}_{L_r(s)\text{ rational and strictly proper}} + \underbrace{V_O T_O\left(1 - \mathrm{e}^{-s\xi_{cam}}\left(1 - \mathrm{e}^{-s\tilde{\xi}_{cam}}\right)\right) - \frac{V_O}{s}\mathrm{e}^{-s\xi_{cam}}\left(1 - \mathrm{e}^{-s\tilde{\xi}_{cam}}\right)}_{L_a(s)\in\hat{\mathcal{A}}}. \tag{28}$$

Second, $1 + L(s)$ has to be analyzed. Suppose that $L(s)$ has p poles in $\mathbb{C}_0^+$. Here, $\mathbb{C}_0^+$ denotes the right half of the complex plane, i.e. $\mathbb{C}_0^+ = \{s \in \mathbb{C} : \Re\{s\} > 0\}$, with $\Re\{\cdot\}$ denoting the real part. Let $\bar{N}_\infty$ be the so-called *Nyquist contour*, which is the semi-circle contour encompassing $\mathbb{C}_0^+$ in the clockwise sense. This semi-circle has an infinite radius and its straight section is generally the $j\omega$-axis (imaginary axis). However, if $L(s)$ features poles on the $j\omega$-axis, small *detours* around these poles have to be made. These detours are small semi-circles in the counterclockwise direction around these poles (so that the detours are in $\mathbb{C}_0^+$). The radius of the detours is infinitesimally small, meaning that they do not exclude any relevant part of $\mathbb{C}_0^+$. Based on these definitions, the second part of the Nyquist-like stability test requires that

$$1 + L(s) \neq 0 \quad \forall s \in \bar{N}_\infty$$

and that $1 + L(s)|_{s\in\bar{N}_\infty}$ encircles the origin ($s = 0$) p times in the counterclockwise sense.

From (28), it follows that $p = 0$. Therefore,

$$\Re\{1 + L(s)\} > 0 \quad \forall s \in \bar{N}_\infty \tag{29}$$

implies that the second part of the above stability test is satisfied. Because (29) is sufficient but generally not necessary for the second part of the stability test, (29) may yield an overly conservative (yet safe) approximation of the true stability region. However, for the proposed outer loop, (29) is a tractable stability test.

The following statement is shown in Appendix A. For satisfaction of (29) with $L(s)$ from (27) it is sufficient (though not necessary) that $V_O > 0$, $T_O > 0$, and

$$\frac{1}{V_O} + T_O > \underbrace{2\left|\sin\left(\omega\frac{\tilde{\xi}_{cam}}{2}\right)\right|\sqrt{T_O^2 + \frac{1}{\omega^2}}}_{rhs(\omega)} \quad \forall\omega \in \mathbb{R}.$$

The global maximum of $rhs(\omega)$ occurs, see Appendix B, at the point

$$\omega = \begin{cases} 0 & \text{if } T_O \leq \frac{|\tilde{\xi}_{cam}|}{2\sqrt{3}} \\ \pm\omega^* & \text{otherwise} \end{cases},$$

where ω^* is the smallest strictly positive solution of

$$0 = \left(\frac{\tilde{\xi}_{cam}\omega^*}{2}\right)^3\left(\frac{2T_O}{\tilde{\xi}_{cam}}\right)^2 + \frac{\tilde{\xi}_{cam}\omega^*}{2} - \tan\left(\frac{\tilde{\xi}_{cam}\omega^*}{2}\right).$$

The values ω^* and $rhs(\omega)$ have to be numerically computed whereas $rhs(0) = |\tilde{\xi}_{cam}|$. These results show which conditions the tuning parameters V_O and T_O have to satisfy for robust closed-loop stability and conclude the stability analysis.

From (26), the tracking error of the outer loop follows in the form

$$\hat{e}_O(s) = \hat{y}_{2,ref}(s) - \hat{y}_2(s) = \frac{1}{1 + L(s)}\mathbf{E}(s)\begin{bmatrix}\hat{y}_{2,ref}(s)\\ \hat{d}_2(s)\\ \hat{u}_3(s)\\ \hat{u}_4(s)\end{bmatrix}$$

with the abbreviation

$$\mathbf{E}(s) = \begin{bmatrix} 1 - \mathrm{e}^{-s\tilde{\xi}_{cam}} + C_O(s)(1 - \mathrm{e}^{-s\xi_{cam}}) \\ \left(C_O(s)(\mathrm{e}^{-s\xi_{cam}} - 1) - 1\right)\mathrm{e}^{-s\tilde{\xi}_{cam}} \\ -\tilde{A}_3\left(C_O(s)(\mathrm{e}^{-s\xi_{cam}} - 1) - 1\right)\mathrm{e}^{-s\tilde{\xi}_{cam}} \\ \tilde{A}_3\left(2A_3 + \tilde{A}_3\right)\left(C_O(s)(\mathrm{e}^{-s\xi_{cam}} - 1) - 1\right)\mathrm{e}^{-s\tilde{\xi}_{cam}} \end{bmatrix}^{\mathrm{T}}.$$

Using the final value theorem, it follows that

$$\lim_{X\to\infty} e_O(X) = \lim_{s\to 0} s\hat{e}_O(s) = 0$$

for constant inputs $y_{2,ref}$, d_2, u_3, and u_4, i.e., $\hat{y}_{2,ref}(s) = \frac{1}{s}\alpha_0$, $\hat{d}_2(s) = \frac{1}{s}\alpha_1$, $\hat{u}_3(s) = \frac{1}{s}\alpha_2$, and $\hat{u}_4(s) = \frac{1}{s}\alpha_3$ with arbitrary constants $\alpha_i \in \mathbb{R}$, $i = 0, 1, 2, 3$. The steady-state error vanishes in this case.

C. Implementation

The discussed feedback control laws are parameterized as functions of the processed plate length X. However, the angular and longitudinal velocities as well as the curvature of the plate are measured with a fixed sampling time $T_{s,fb}$. This is why the controllers are implemented in a discrete-time form. Assuming piecewise constant inputs and using the Euler-forward integration scheme for a sampling period $kT_{s,fb} \leq t < (k+1)T_{s,fb}$, the PI-feedback control law of the inner loop at $t = kT_{s,fb}$ follows in the form

$$u_{1,fb}(kT_{s,fb}) = \frac{V_I}{A_1}T_I\left(y_{1,ref}(kT_{s,fb}) - y_1(kT_{s,fb})\right) + \frac{V_I}{A_1}x_{I,k}, \tag{30}$$

with the update of the discrete-time integrator state

$$x_{I,k+1} = x_{I,k} + \bar{v}^{out}(kT_{s,fb})T_{s,fb}\left(y_{1,ref}(kT_{s,fb}) - y_1(kT_{s,fb})\right).$$

The spatial increment $X_{k+1} - X_k = \bar{v}^{out}\left(kT_{s,fb}\right)T_{s,fb}$ follows directly from (14). By analogy, the PI control law for the outer loop reads as

$$y_{1,fb}(kT_{s,fb}) = V_O T_O \tilde{e}_O(kT_{s,fb}) + V_O x_{O,k}, \tag{31}$$

with the update of the discrete-time integrator state

$$x_{O,k+1} = x_{O,k} + \bar{v}^{out}(kT_{s,fb})T_{s,fb}\tilde{e}_O(kT_{s,fb}).$$

The initial states of the integrators are set to $x_{I,0} = x_{O,0} = 0$. Clearly, the sampling time $T_{s,fb}$ must not be too large to ensure a sufficient approximation of the initial continuous control laws. Additionally, if $T_{s,fb}$ is chosen too large the internal stability of the system may be lost.

The feedback part $u_{1,fb}$ of the inner control loop is limited to $u_{1,min} \leq u_{1,fb} \leq u_{1,max}$ to avoid an excessive (additional) asymmetry of the output thickness of the plate. In combination with the integrators used in the feedback controllers, such a constraint of the control input can lead to a windup behavior

Post-print version of the article: F. Schausberger, A. Steinboeck, and Kugi, "Feedback control of the contour shape in heavy-plate hot rolling," *IEEE Transactions on Control Systems Technology*, vol. 26, no. 3, pp. 842–856, 2018. DOI: 10.1109/TCST.2017.2695168
The content of this post-print version is identical to the published paper but without the publisher's final layout or copy editing.

of the controller, which is associated with a deterioration of the control performance. This is why a simple anti-windup scheme called conditional integration, see, e.g., [34], is added to the control laws (30) and (31). The integrator state $x_{I,k}$ is only updated if one of the conditions

$$
\begin{gathered}
u_{1,min} < u_{1,fb}(kT_{s,fb}) < u_{1,max} \\
u_{1,fb}(kT_{s,fb}) \leq u_{1,min} \wedge y_{1,ref}(kT_{s,fb}) > y_1(kT_{s,fb}) \\
u_{1,fb}(kT_{s,fb}) \geq u_{1,max} \wedge y_{1,ref}(kT_{s,fb}) < y_1(kT_{s,fb})
\end{gathered}
$$

is fulfilled. Otherwise, the integrator state is held constant. The first condition ensures that the integrator of the inner controller is updated if the control input $u_{1,fb}(kT_{s,fb})$ is within the given limits $u_{1,min}$ and $u_{1,max}$. The second condition is fulfilled if the control input is below or equal to the lower limit $u_{1,min}$ and the control error $e_I(kT_{s,fb}) = y_{1,ref}(kT_{s,fb}) - y_1(kT_{s,fb})$ is positive. Hence, in case of an active lower constraint the update is only performed when the violation of $u_{1,min}$ will be reduced. Similarly, condition three should help to reduce the violation of the limit $u_{1,max}$.

The input $y_{1,ref}$ of the outer control loop is not subject to a limitation. However, an active constraint of the input u_1 of the inner control should also be considered in the outer control loop. Assume that the lower constraint of the inner loop is active, i.e. $u_{1,fb}(kT_{s,fb}) \leq u_{1,min}$, then a further decrease of the reference value of the inner loop $y_{1,ref}(kT_{s,fb})$ should be avoided. Hence, the integrator state $x_{O,k}$ is only updated if the control error of the outer loop is positive which leads to an increase of $y_{1,ref}(kT_{s,fb})$. Analogously, if the upper constraint is active, i.e. $u_{1,fb}(kT_{s,fb}) \geq u_{1,max}$, the integrator state $x_{O,k}$ is only updated if the control error of the outer loop is negative.

Consequently, the integrator state $x_{O,k}$ is only updated for

$$
\begin{gathered}
u_{1,min} < u_{1,fb}(kT_{s,fb}) < u_{1,max} \\
u_{1,fb}(kT_{s,fb}) \leq u_{1,min} \wedge \tilde{e}_O(kT_{s,fb}) > 0 \\
u_{1,fb}(kT_{s,fb}) \geq u_{1,max} \wedge \tilde{e}_O(kT_{s,fb}) < 0.
\end{gathered}
$$

Here, the first condition represents the case where no constraint of the inner control input is violated. The second and third condition should help to reduce the violation of an active lower or upper constraint, respectively.

V. Simulations and measurements

In the following section, the impact of disturbances and parameter uncertainties on the proposed feedback control approach from Sec. IV is studied by means of simulations. Furthermore, measurements from the considered mill stand demonstrate the effectivity of the proposed method.

A. Simulation results

The last pass of a plate with a final plate length of 31.7 m and a width of $w = 2.59$ m is considered in the simulations. The plate thickness is reduced during the considered pass from 15.1 mm to the final plate thickness of 13.1 mm. A rectangular shape before the rolling pass and a homogeneous input thickness profile ($\Delta h^{in} = 0$) are presumed. Hence, the feedforward part of the asymmetry vanishes, i.e., $u_{1,ff} = 0$. A long and thin plate was chosen because from experience it is known that such plates tend to camber during the rolling process.

The mathematical model of the movement of the plate (19) is used to simulate the contour evolution in the considered pass. The input and the output thickness profiles as well as the centerline of the plate before the rolling pass are fed to the mathematical model (19a) and (19b) and the outputs (19c) and (19d) are used in the feedback controller.

TABLE I
Parameters used for the simulations of the feedback controller.

Parameter	Value	Unit
V_I	0.5	m^{-1}
T_I	0	m
V_O	0.4	m^{-1}
T_O	0.1	m
$T_{s,cm}$	33	ms
$T_{s,fb}$	100	ms
$u_{1,min}$	-100	µm
$u_{1,max}$	100	µm
ξ_{cam}	5	m
X_{min}	9	m

The plate is rolled with a constant rolling speed $\bar{v}^{out} = 3$ m/s in forward direction. Furthermore, it is assumed that the upstream angular displacement vanishes, i.e., $\Omega^{in} = 0$ (cf. Fig. 6) because the upstream side guides are closed. A non-ideal control of the rolling gap actuator is considered by choosing $d_1 = A_1 \Delta u_1$ where $\Delta u_1 = 20$ µm represents a constant disturbance of the asymmetry of the output thickness. The disturbance d_2 and the constants $\tilde{A}_1$, $\tilde{A}_2$, and $\tilde{A}_3$ are set to zero. The centerline and the movement of the plate are measured with the sampling time $T_{s,cm} = 33$ ms which is also used by the infrared cameras. However, the sampling time of the discrete time controller is set to $T_{s,fb} = 100$ ms because the desired asymmetry of the output thickness can only be changed every 100 ms at the considered rolling mill. The controller parameters shown in Tab. I were empirically determined on the mill stand during a commissioning phase with different types of plates. According to the stability analysis from Sec. IV-B2, the parameters used for the outer controller ensure internal stability for $|\tilde{\xi}_{cam}| < 2.6$ m. In the simulations $\tilde{\xi}_{cam} = 0$ m is used.

Because a central control objective is a straight plate, the desired curvature is set to $y_{2,ref} = 0$. The FOVs of the cameras are located $\xi_{cam} = 5$ m away from the rolling gap. The plate must range a few meters into the FOV for a reliable measurement of the contour and the movement of the plate. Therefore, a rolled plate length larger than the constant X_{min} (cf. [25]) is necessary to measure the downstream angular displacement. Hence, the feedback controller is activated when the minimum rolled plate length X_{min} is reached, i.e., $X > X_{min}$ is satisfied for the first time.

Fig. 12 shows the simulation results without and with applying the feedback controller. The centerlines shown in the upper part of this figure are centered in longitudinal direction and rotated such that the slope $(\delta^{out})'$ vanishes at $x = 0$ m.

Post-print version of the article: F. Schausberger, A. Steinboeck, and Kugi, “Feedback control of the contour shape in heavy-plate hot rolling,” *IEEE Transactions on Control Systems Technology*, vol. 26, no. 3, pp. 842–856, 2018. doi: 10.1109/TCST.2017.2695168
The content of this post-print version is identical to the published paper but without the publisher’s final layout or copy editing.

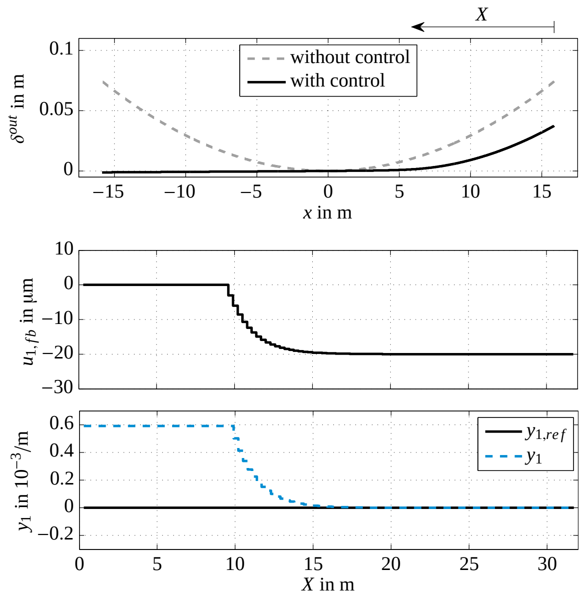

Fig. 12. Simulation results of the feedback control approach with $d_2 = 0$.

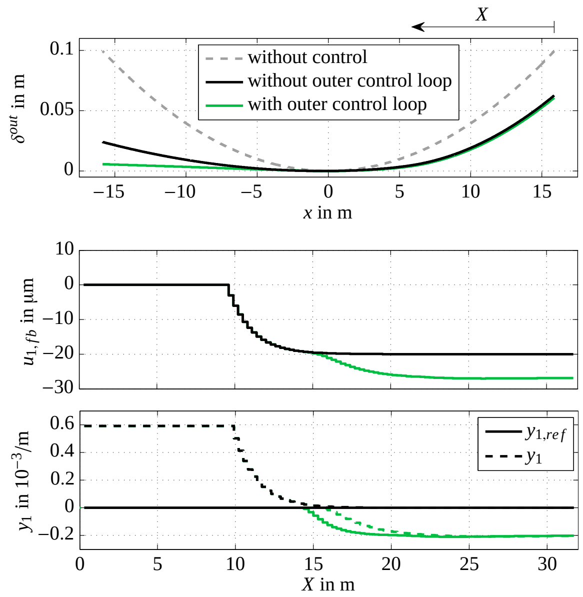

Fig. 13. Simulation results of the feedback control approach with $d_2 = 0.2 \cdot 10^{-3}$/m with and without using the outer control loop.

For $X < X_{min}$, the camber of the plate cannot be reduced since a measurement of the downstream plate is not available at this time. However, for the remaining part of the plate, i.e., $X \geq X_{min}$, the curvature can be reduced to almost zero. As shown in Fig. 12, the necessary control effort in form of the output asymmetry is in the range of 20 µm. The lower part of Fig. 12 shows that the controller of the inner loop ensures $y_{1,ref} = y_1$ within a few meters after the activation of the feedback controller. The outer controller should not be activated until $y_{1,ref} = y_1$ is sufficiently ensured because otherwise the prerequisite of an ideal inner control loop is not fulfilled. For the parameters used in the inner controller, activating the outer controller for $X \geq X_{min} + 6$ m has proven to be useful. The control effort $y_{1,ref}$ of the outer control loop stays almost constant after the activation of the controller. The tolerable overcompensation of the curvature of the centerline seen in the upper part of Fig. 12 results from the non-ideal inner control loop which is not incorporated into the design of the outer controller.

The second simulation scenario is similar to the first one but uses the constant disturbance $d_2 = 0.2 \cdot 10^{-3}$/m. Fig. 13 shows the simulation results with ($T_O \neq 0$, $V_O \neq 0$) and without ($T_O = 0$, $V_O = 0$) the outer feedback controller C_O. After some distance for the feedback controller to become active ($X \approx 20$ m), the outer loop compensates the effect of the disturbance d_2. By contrast, without using the outer control loop the effect of the disturbance d_2 cannot be suppressed.

B. Measurements

In the following, measurement results from plates rolled at the heavy-plate finishing mill of AG der Dillinger Hüttenwerke are presented. The discussed control strategies and the algorithmic part of the contour measurement system presented in [25] were implemented in C++ and are executed on a standard PC. The data exchange between this PC and the mill stand computer is performed by means of TCP/IP messages.

1) Exemplary plate: The same parameters as in the simulations of the feedback controller are used in the real-time implementation, see Tab. I. The center input and output thickness $\bar{h}^{in}$ and $\bar{h}^{out}$ are set to the desired input and output thickness of the plate, respectively.

The contour measurement has a lower sampling time ($T_{s,cm} = 33$ ms) compared to the sampling time $T_{s,fb} = 100$ ms of the feedback controller. To avoid aliasing effects, the mean value of the quantities measured by the contour measurement within a sampling period $T_{s,fb}$ are used in the feedback controller. At the end of the rolling pass, upstream measurements of the plate are not available due to the distance between the FOV of the camera and the mill stand. If upstream measurements are not available, the upstream quantities $\left(\delta^{in}\right)''$ and Ω^{in} are set to zero in the feedback controller. Fig. 14 shows the results obtained for a plate with a final plate thickness of 12.4 mm and a final plate length of 29.8 m. During this rolling pass, the upstream side guides centered the plate in the lateral direction. The upper part of Fig. 14 shows the centerline of the plate before and after the rolling pass. The centerline before the rolling pass only shows a small camber. However, the plate shows a considerable camber near the head end ($x > 5$ m) after the rolling pass. Nevertheless, the curvature of the downstream centerline has been reduced to almost zero after X_{min} plus a few meters for the controller to become active. Furthermore, Fig. 14 shows the control efforts of the feedforward and the feedback controller $u_{1,ff}$ and $u_{1,fb}$, respectively. The desired and measured downstream angular velocities are shown in the lower part of Fig. 14. For the considered plate, the measurement of the downstream angular velocity is very noisy. However, the proposed control

Post-print version of the article: F. Schausberger, A. Steinboeck, and Kugi, "Feedback control of the contour shape in heavy-plate hot rolling," *IEEE Transactions on Control Systems Technology*, vol. 26, no. 3, pp. 842–856, 2018. DOI: 10.1109/TCST.2017.2695168
The content of this post-print version is identical to the published paper but without the publisher's final layout or copy editing.

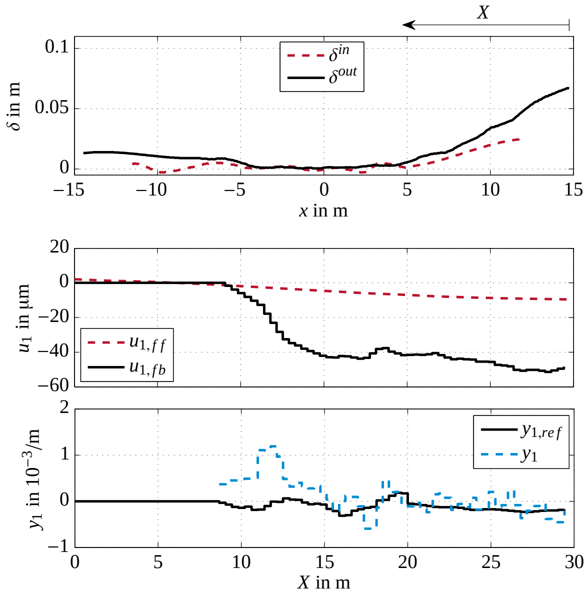

Fig. 14. Measurement results of the feedback control approach applied to the last pass of a 29.8 m long plate.

approach can significantly reduce the camber of the plate even for measurements which are corrupted by large noise.

2) Statistics: The plates are trimmed to rectangular shapes at the end of the production process. Clearly, the usable area of the plates should be maximized. This requirement is equivalent to maximizing the width of the blue region (usable area) inside the plate boundaries shown in Fig. 15 when neglecting the shape of the tail and head end. The maximum width of the usable area is denoted by w^* (cf. Fig. 15) and is determined from the longitudinal boundaries of the plate by means of static optimization. In the following, the difference $\Delta w = w - w^*$ is used as an aggregate measure of the plate width lost due to contour errors.

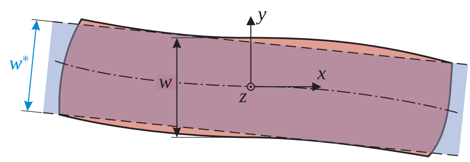

Fig. 15. Plate with contour error and rectangular usable area inside the longitudinal boundaries of the plate.

Fig. 16 shows the frequency distribution of the contour errors obtained without any control and with the feedforward control from [25] in combination with the presented feedback control approach. Thereby, 2600 plates were rolled with camber control switched on and 2600 plates with comparable dimensions and material properties were rolled without any control. The plates used in the comparison have a minimal plate length of 15 m and a maximum final plate thickness of 30 mm. For shorter plates almost no improvement of the contour can be achieved by feedback control because of the minimal plate length $X_{min} = 9$ m associated with the distance between the FOV of the camera and the mill stand.

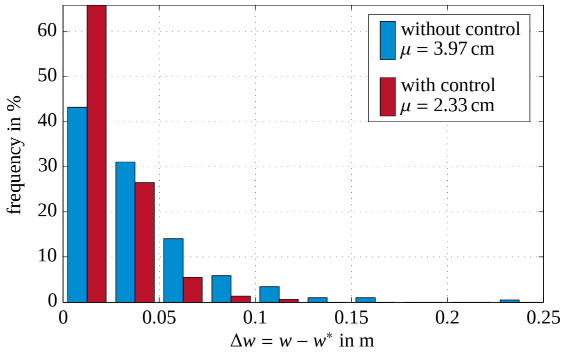

Fig. 16. Frequency distribution of Δw obtained without any control and with feedforward and feedback control (sample size 2600 plates).

Compared to the plates without any camber control, the mean value of Δw has been reduced by approximately 40 % by the feedforward and feedback controller. In comparison, only using the feedforward approach from [25] has led to a reduction of Δw of approximately 20 %. Using both control measures yields $\Delta w < 5$ cm for 92 % of the plates.

VI. Conclusions

In this work, a feedback control approach for the reduction of contour errors in hot rolling of heavy plates was developed. First, a vision-based system for the measurement of the movement and the contour of the plate was shortly revisited. A model describing the nexus between the movement and the evolution of the centerline of the plate during the rolling pass was presented and validated by means of measurements of a plate rolled during the standard production process. The model was used in a feedback control approach to reduce errors between the desired and the actual curvature of the centerline during the rolling pass. In particular, a 2-DOF Smith-predictor controller utilizing the delay-free measurement of the angular velocity was presented. The presented approach differs from the approaches found in literature as the upstream and downstream contour and the movement of the plate are simultaneously measured and utilized in the feedback controller. Simulations and measurement results show that the proposed control approach can significantly reduce contour errors in hot rolling.

Acknowledgment

The authors gratefully acknowledge the financial support and the realization of a pilot installation by Aktiengesellschaft der Dillinger Hüttenwerke, Germany.

Appendix A

For proving BIBO stability of (26), it is sufficient to satisfy

$$\Re\{1 + L(s)\} > 0 \quad \forall s \in \bar{N}_\infty. \tag{32}$$

Post-print version of the article: F. Schausberger, A. Steinboeck, and Kugi, "Feedback control of the contour shape in heavy-plate hot rolling," *IEEE Transactions on Control Systems Technology*, vol. 26, no. 3, pp. 842–856, 2018. doi: 10.1109/TCST.2017.2695168
The content of this post-print version is identical to the published paper but without the publisher's final layout or copy editing.

Insertion of $L(s)$ from (27) into (32) and evaluation along the $j\omega$-axis yields

$$\frac{1}{V_O} + \frac{1}{\omega}\left[\sin(\omega\xi_{cam}) - \sin(\omega\bar{\xi}_{cam})\right] + T_O\left[1 - \cos(\omega\xi_{cam}) + \cos(\omega\bar{\xi}_{cam})\right] > 0.$$

Applying the summation formulas for trigonometric functions results in

$$\frac{1}{V_O} + T_O > 2T_O \sin\left(\frac{\omega(2\xi_{cam} + \tilde{\xi}_{cam})}{2}\right)\sin\left(\frac{\omega\tilde{\xi}_{cam}}{2}\right) + \frac{2}{\omega}\cos\left(\frac{\omega(2\xi_{cam} + \tilde{\xi}_{cam})}{2}\right)\sin\left(\frac{\omega\tilde{\xi}_{cam}}{2}\right). \quad (33)$$

Using Pythagoras' theorem, an upper bound of the right-hand side of (33) is found in the form

$$2\left|\sin\left(\frac{\omega\tilde{\xi}_{cam}}{2}\right)\right|\sqrt{T_O^2 + \frac{1}{\omega^2}}.$$

Hence,

$$\frac{1}{V_O} + T_O > 2\left|\sin\left(\frac{\omega\tilde{\xi}_{cam}}{2}\right)\right|\sqrt{T_O^2 + \frac{1}{\omega^2}}$$

ensures internal stability of (26).

Appendix B

The task is to determine the global maximum of

$$rhs(\omega) = 2\left|\sin\left(\omega\frac{\tilde{\xi}_{cam}}{2}\right)\right|\sqrt{T_O^2 + \frac{1}{\omega^2}} \quad (34)$$

with respect to ω. Note that (34) is symmetric in ω. The maximum of $rhs(\omega)$ is found by analyzing the roots ω^* of $\frac{\mathrm{d}rhs(\omega)}{\mathrm{d}\omega}\Big|_{\omega=\omega^*}$. The roots ω^* follow from solving the equation

$$0 = \left(\frac{\tilde{\xi}_{cam}\omega^*}{2}\right)^3\left(\frac{2T_O}{\tilde{\xi}_{cam}}\right)^2 + \frac{\tilde{\xi}_{cam}\omega^*}{2} - \tan\left(\frac{\tilde{\xi}_{cam}\omega^*}{2}\right). \quad (35)$$

Utilizing the Taylor series expansion of $\tan(x)$ about 0, i.e., $\tan(x) = x + \frac{1}{3}x^3 + \frac{2}{15}x^5 + \frac{17}{315}x^7 + \ldots$, (35) may be written in the specialized form

$$0 = \left(\frac{\tilde{\xi}_{cam}\omega^*}{2}\right)^3 \left[\underbrace{\left(\frac{2T_O}{\tilde{\xi}_{cam}}\right)^2 - \frac{1}{3}}_{k_1}\underbrace{- \frac{2}{15}\left(\frac{\tilde{\xi}_{cam}\omega^*}{2}\right)^2 - \frac{17}{315}\left(\frac{\tilde{\xi}_{cam}\omega^*}{2}\right)^4 - \ldots}_{k_2(\omega^*)}\right]. \quad (36)$$

Clearly, $\omega^* = 0$ is a solution of (36). Because of $k_2(\omega^*) \le 0$, an additional solution of (35) exists for $k_1 > 0$, i.e., if $T_O > \frac{|\tilde{\xi}_{cam}|}{2\sqrt{3}}$.

The solution $\omega^* = 0$ only represents a maximum of $rhs(\omega)$ if $T_O \le \frac{|\tilde{\xi}_{cam}|}{2\sqrt{3}}$ because then

$$\frac{\mathrm{d}^2 rhs(\omega)}{\mathrm{d}\omega^2}\bigg|_{\omega=0} = \frac{1}{12}\left|\tilde{\xi}_{cam}\right|\left(12T_O^2 - \tilde{\xi}_{cam}^2\right)$$

is non-positive. For $T_O > \frac{|\tilde{\xi}_{cam}|}{2\sqrt{3}}$, the global maximum occurs at $\omega = \pm\omega^*$ where ω^* is the smallest strictly positive solution of (35).

References

[1] T. Ishikawa, Y. Tozawa, and J. Nishizawa, "Fundamental study on snaking in strip rolling," *Trans. Iron Steel Inst. Japan*, vol. 28, no. 6, pp. 485–490, 1988.

[2] J. Canny, "A computational approach to edge detection," *IEEE Trans. on Pattern Anal. and Mach. Intell.*, vol. 8, pp. 679–698, 1986.

[3] B. N. Carruthers-Watt, Y. Xue, and A. J. Morris, "A vision based system for strip tracking measurement in the finishing train of a hot strip mill," in *Proc. IEEE ICMA 2010*, Xi'an, China, August 2010, pp. 1115–1120.

[4] R. J. Montague, J. Watton, and K. J. Brown, "A machine vision measurement of slab camber in hot strip rolling," *J. Mater. Proc. Tech.*, vol. 168, pp. 172–180, 2005.

[5] A. Ollikkala, T. Kananen, A. Mäkynen, M. Holappa, E. Torppa, and T. Harvala, "A single camera system for camber measurement in hot strip rolling," in *Proc. Rolling 2013 - 9th Int. Rolling Conf. and 6th European Rolling Conf.*, Venice, Italy, June 2013.

[6] R. C. González, R. Valdés, and J. A. Cancelas, "Vision based measurement system to quantify straightness defect in steel sheets," in *9th Int. Conf. Comput. Anal. of Images and Patterns*, Warsaw, Poland, September 2001, pp. 427–434.

[7] J. W. Yoo, N. W. Kong, J. Song, and P. G. Park, "Camber detection algorithm using the image stitching technique in hot-rolling process," in *Int. Conf. Robotics*, Phuket, Thailand, November 2010, pp. 74–77.

[8] J. Lee, N. Kong, J. Yoo, and P. Park, "A fast image stitching algorithm in the endless hot rolling process," in *11th Int. Conf. on Control, Automation and Syst.*, Gyeonggi-do, Korea, October 2011, pp. 1264–1268.

[9] N. W. Kong, J. W. Yoo, J. S. Lee, S. W. Yun, J. Bae, and P. G. Park, "Vision-based camber measurement system in the endless hot rolling process," *Opt. Eng.*, vol. 50, no. 10, pp. 107 202–1–107 202–10, 2011.

[10] T. Shiraishi, H. Ibata, A. Mizuta, S. Nomura, E. Yoneda, and K. Hirata, "Relation between camber and wedge in flat rolling under restrictions of lateral movement," *Iron Steel Inst. Japan Int.*, vol. 31, no. 6, pp. 583–587, 1991.

[11] A. Nilsson, "FE simulations of camber in hot strip rolling," *J. Mater. Proc. Tech.*, vol. 80–81, pp. 325–329, 1998.

[12] D. L. Biggs, S. J. Hardy, and K. J. Brown, "Finite element modelling of camber development during hot rolling of strip steel," *Ironmak. and Steelmak.*, vol. 25, no. 1, pp. 81–89, 1998.

[13] M. Trull, D. McDonald, A. Richardson, and D. C. J. Farrugia, "Advanced finite element modelling of plate rolling operations," *J. Mater. Proc. Tech.*, vol. 177, pp. 513–516, 2006.

[14] A. Dixon and D. Yuen, "Mathematical analysis of the effects of width-wise asymmetric rolling conditions on head-end wedge, camber and off-centre," in *Rolling 2013 - 9th Int. Rolling Conf. and 6th European Rolling Conf.*, Venice, Italy, June 2013.

[15] J. H. Ruan, L. W. Zhang, S. D. Gu, W. B. He, and S. H. Chen, "3D FE modelling of plate shape during heavy plate rolling," *Ironmak. and Steelmak.*, vol. 41, no. 3, pp. 199–205, 2014.

[16] I. Malloci, J. Daafouz, C. Iung, R. Bonidal, and P. Szczepanski, "Robust steering control of hot strip milling," *IEEE Trans. Control Syst. Technol.*, vol. 18, no. 4, pp. 908–917, 2010.

[17] T. Kiyota, H. Matsumoto, Y. Adachi, E. Kondo, Y. Tsuji, and S. Aso, "Tail crash control in hot strip mill by LQR," in *Proc. Amer. Control Conf.*, Denver, Colorado, June 2003, pp. 3049–3054.

[18] M. Okada, K. Murayama, Y. Anabuki, and Y. Hayashi, "VSS control of strip steering for hot rolling mills," in *Proc. 16th IFAC World Congress*, Prague, Czech Republic, July 2005, pp. 1681–1686.

[19] I. Choi, J. Rossiter, J. Chung, and P. Fleming, "An MPC strategy for hot rolling mills and applications to strip threading control problems," in *Proc. 17th IFAC World Congress*, Seoul, Korea, July 2008, pp. 1661–1662.

[20] Y. J. Choi and M. C. Lee, "PID sliding mode control for steering of lateral moving strip in hot strip rolling," *Int. J. Control, Automation and Syst.*, vol. 7, no. 3, pp. 399–407, 2009.

[21] C. W. J. Hol, J. de Roo, L. Kampmeijer, T. Dirkson, G. Schipper, M. L. Maire, and J. van der Lugt, "Model predictive controller for strip-tracking during tail-out of the finishing mill," in *Proc. IFAC MMM 2013*, San Diego, USA, August 2013, pp. 397–402.

[22] Y. Tanaka, K. Omori, T. Miyake, K. Nishizaki, M. Inoue, and S. Tezuka, "Camber control techniques in plate rolling," Kawasaki Steel, Tech. Rep. 16, June 1987.

[23] D. Jeong, Y. Kang, Y. J. Jang, D. Lee, and S. Won, "Development of FEM simulator combined with camber reducing output feedback fuzzy controller for rough rolling process," *Iron Steel Inst. Japan Int.*, vol. 53, no. 3, pp. 511–519, 2013.

Post-print version of the article: F. Schausberger, A. Steinboeck, and Kugi, "Feedback control of the contour shape in heavy-plate hot rolling," *IEEE Transactions on Control Systems Technology*, vol. 26, no. 3, pp. 842–856, 2018. doi: 10.1109/TCST.2017.2695168
The content of this post-print version is identical to the published paper but without the publisher's final layout or copy editing.

[24] F. Schausberger, A. Steinboeck, and A. Kugi, "Optimization-based reduction of contour errors of heavy plates in hot rolling," *Journal of Process Control*, vol. 47, pp. 150–160, 2016.
[25] ——, "Optimization-based estimator for the contour and movement of heavy plates in hot rolling," *J. Process Control*, vol. 29, pp. 23–32, 2015.
[26] F. Schausberger, K. Speicher, A. Steinboeck, M. Jochum, and A. Kugi, "Two illustrative examples to show the potential of thermography for process monitoring and control in hot rolling," in *Proc. 16th IFAC MMM*, Oulu, Finland, August 2015, pp. 48–53.
[27] J. G. Lenard, *Primer on Flat Rolling*, 2nd ed. Oxford: Elsevier, 2014.
[28] K. H. Weber, "Hydrodynamic theory of rolling," *J. Iron Steel Inst.*, vol. 203, pp. 27–35, 1965.
[29] F. Schausberger, A. Steinboeck, and A. Kugi, "Mathematical modeling of the contour evolution of heavy plates in hot rolling," *Appl. Math. Modell.*, vol. 39, no. 15, pp. 4534–4547, 2015.
[30] N. Abe and K. Yamanaka, "Smith predictor control and internal model control - A tutorial," in *Proc. IEEE SICE*, Fukui, Japan, August 2003, pp. 1383–1387.
[31] J. E. Normey-Rico and E. F. Camacho, *Control of Dead-time Processes*. London: Springer, 2007.
[32] M. Vidyasagar, *Nonlinear Systems Analysis*, 2nd ed., ser. Classics in Applied Mathematics. Philadelphia: SIAM, 1992, no. 42.
[33] R. F. Curtain and H. Zwart, *An Introduction to Infinite-dimensional Linear Systems Theory*. New York: Springer, 1995, vol. 21 *of Texts in Applied Mathematics*.
[34] A. Visioli, *Practical PID Control*, ser. Advances in Industrial Control. London: Springer, 2006.

Florian Schausberger received the Dipl.-Ing. degree in mechatronics from Johannes Kepler University, Linz, Austria, in 2011, and the Ph.D. (Dr. techn.) degree in electrical engineering from Vienna University of Technology, Austria, in 2016.

From 2012 to 2016 he was a research assistant with the Automation and Control Institute at TU Wien, Vienna, Austria. His main research interests cover the mathematical modeling of nonlinear dynamical systems and the model-based observer and controller design with focus on rolling mill automation.

Andreas Steinboeck received the M.Sc. degree in mechatronics from Loughborough University, Loughborough, U.K., in 2005, the Dipl.-Ing. degree in mechatronics from Johannes Kepler University, Linz, Austria, in 2007, and the Ph.D. (Dr. techn.) degree in electrical engineering from Vienna University of Technology, Austria, in 2011.

Since 2007, he has been a research assistant with the Automation and Control Institute at TU Wien, Vienna, Austria. His main research interests cover numerical methods in engineering, mechanical structures, stability analysis, mathematical modeling, identification, optimization and control of nonlinear dynamical systems, as well as applications in continuous production processes in the steel industry.

Andreas Kugi (M'94) received the Dipl.-Ing. degree in electrical engineering from Graz University of Technology, Austria, and the Ph.D. (Dr. techn.) degree in control engineering from Johannes Kepler University (JKU), Linz, Austria, in 1992 and 1995, respectively. He received his Habilitation degree in the field of automatic control and control theory from JKU in 2000.

From 1995 to 2000 he worked as an assistant professor and from 2000 to 2002 as an associate professor at JKU. In 2002, he was appointed full professor at Saarland University, Saarbrücken, Germany, where he held the Chair of System Theory and Automatic Control until May 2007. Since June 2007 he is a full professor for complex dynamical systems and head of the Automation and Control Institute (ACIN) at TU Wien, Vienna, Austria. His research interests include the physics-based mathematical modeling, control and optimization of nonlinear dynamical systems with a strong focus on industrial applications.

Dr. Kugi is full member of the Austrian Academy of Sciences and Editor-in-Chief of the Control Engineering Practice.

Post-print version of the article: F. Schausberger, A. Steinboeck, and Kugi, "Feedback control of the contour shape in heavy-plate hot rolling," *IEEE Transactions on Control Systems Technology*, vol. 26, no. 3, pp. 842–856, 2018. DOI: 10.1109/TCST.2017.2695168
The content of this post-print version is identical to the published paper but without the publisher's final layout or copy editing.